

Joint Routing, Resource Allocation, and Energy Optimization for Integrated Access and Backhaul with Open RAN

Reshma Prasad*, Maxime Elkael*, Gabriele Gemmi, Osama M. Bushnaq, Debashisha Mishra,
Prasanna Raut, Jennifer Simonjan, Michele Polese, Tommaso Melodia

Abstract—As networks evolve towards 6G, Mobile Network Operators (MNOs) must accommodate diverse requirements and at the same time manage rising energy consumption. Integrated Access and Backhaul (IAB) networks facilitate dense cellular deployments with reduced infrastructure complexity. However, the multi-hop wireless backhauling in IAB networks necessitates proper routing and resource allocation decisions to meet the performance requirements. At the same time, cell densification makes energy optimization crucial. This paper addresses the joint optimization of routing and resource allocation in IAB networks through two distinct objectives: energy minimization and throughput maximization. We develop a novel capacity model that links power levels to achievable data rates. We propose two practical large-scale approaches to solve the optimization problems and leverage the closed-loop control framework introduced by the Open Radio Access Network (O-RAN) architecture to integrate the solutions. The approaches are evaluated on diverse scenarios built upon open data of two months of traffic collected by network operators in the city of Milan, Italy. Results show that the proposed approaches effectively reduces number of activated nodes to save energy and achieves ~ 100 Mbps of minimum data rate per User Equipment (UE) during peak hours of the day using spectrum within the Frequency Range (FR) 3, or upper midband. The results validate the practical applicability of our framework for next-generation IAB network deployment and optimization.

Index Terms—IAB, Open RAN, Optimization, Energy

I. INTRODUCTION

Future wireless networks must address the challenge of supporting a massive number of connected devices while meeting stringent data rate requirements [1], [2]. Integrated Access and Backhaul (IAB) was introduced in 3GPP Release 16 as a cost-effective deployment solution that enables flexible network densification. IAB enables flexible deployment of Next Generation Node Bases (gNBs) called IAB-nodes that rely on in-band wireless communications to connect to a set of gNBs called IAB-donors with wired backhaul links.

This work has been submitted to the IEEE for possible publication. Copyright may be transferred without notice, after which this version may no longer be accessible.

R. Prasad, M. Elkael, G. Gemmi, M. Polese, and T. Melodia are with the Institute for the Wireless Internet of Things, Northeastern University, Boston, MA 02115. Email: {re.prasad, m.elkael, g.gemmi, m.polese, melodia}@northeastern.edu.

O. Bushnaq, D. Mishra, P. Raut, and J. Simonjan are with the Technology Innovation Institute Abu Dhabi, United Arab Emirates. Email: name.surname@tii.ae.

*The authors contributed equally.

This article is based upon work partially supported by the Cooperative Networked UAVs project funded by Technology Innovation Institute and by OUSD(R&E) through Army Research Laboratory Cooperative Agreement Number W911NF-24-2-0065. The views and conclusions contained in this document are those of the authors and should not be interpreted as representing the official policies, either expressed or implied, of the Army Research Laboratory or the U.S. Government. The U.S. Government is authorized to reproduce and distribute reprints for Government purposes notwithstanding any copyright notation herein.

Thus, IAB reduces infrastructure costs and deployment complexity compared to traditional fiber-based solutions [3].

As end-to-end performance of the network depends on number of hops between donor and the User Equipment (UE), the route selection, and the resource allocation, it is necessary to jointly optimize IAB-network topology, routing, and resource allocation to achieve optimal performance [3], [4]. Beyond these optimization aspects, energy-aware network management is crucial for sustainable IAB network management [5]. Fixed IAB nodes enable long-term network planning; however, they do not need to remain active continuously. Instead, they can be selectively activated based on network load, helping to minimize energy consumption. As shown in [6]–[8], dynamically activating and deactivating gNBs with respect to the current load of the network reduces the energy footprint of the system. Power control is another aspect which is crucial for energy optimization, as nodes operating at optimal power levels decrease overall energy consumption. Additionally, power control is essential for interference management, which can affect network capacity. Consequently, the underlying capacity model becomes more dynamic and complex, necessitating a more nuanced optimization approach.

The implementation of these comprehensive optimization strategies requires flexible and programmable network architectures. Such capabilities are enabled by the Radio Access Network (RAN) flexibility and programmability introduced by O-RAN ALLIANCE and the extension of O-RAN architecture to support IAB networks proposed in [9]. The O-RAN architecture allows seamless integration of optimization logic directly into the RAN by exposing interfaces such as E2 and O1, and enabling intelligent closed-loop control via the RAN Intelligent Controller (RIC) [10].

A. Related Works

In recent years, the topic of IAB topology optimization and routing has been of significant interest to the research community. Recent works include genetic algorithms for throughput and coverage optimization in millimeter wave (mmWave) IAB [11], dynamic programming for capacity optimization [12] and reinforcement learning for latency optimization [4]. In [13], the problem is modeled as a multi-commodity flow problem [14] which is solved by a combination of machine learning and linear programming. Though the work focuses on throughput maximization and considers routing, it overlooks power control, which is a critical factor that impacts the achievable data rate. Similarly, [15] explores connection management and throughput maximization in O-RAN architectures leveraging deep reinforcement learning. However, rather than IAB networks, the work focuses on traditional cellular networks.

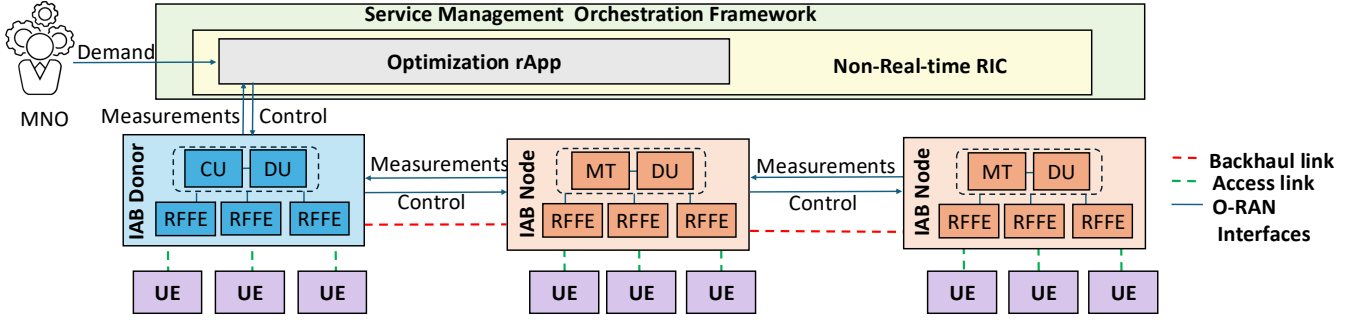


Fig. 1: Example of an IAB Network optimized by O-RAN components. Each IAB-node includes a baseband unit (Distributed Unit (DU) and Mobile Termination (MT)) and Radio Frequency (RF) frontends (RFFEs).

On the other hand, energy efficiency of cellular networks is a long-standing concern, with various works typically tackling the problem through techniques such as power allocation [16], [17], sleep mode optimization [18], and leveraging network heterogeneity [19]. Recently, a few works have explored IAB topology optimization with energy-related objectives. This mainly includes [20], where the problem is modeled considering beamforming and using the Shannon capacity model. The authors then formulate a mixed integer non-linear program, which they solve heuristically by reformulating the objective function, using continuous relaxations and a greedy algorithm. However, the work does not consider dynamic activation/deactivation of IAB-nodes, enabling sleep mode optimization. Though the authors develop a detailed interference model, the use of Shannon capacity leads to theoretical upper bounds on achievable data rates. Other important works on energy optimization include [21] where energy-efficiency is optimized with respect to the Age-of-Information, and our previous work [7] where the topology is optimized for energy in a simplified model which does not consider power allocation and interference.

A concept related to IAB is that of mesh and wireless sensor networks, where a set of sensors (typically Internet of Things (IoT) devices) are directly interconnected via wireless links, without a central entity such as the gNB to coordinate the communication. In that context, numerous papers tackle energy efficiency [22]–[24]. However, the optimization task typically is very different from IAB, as these networks are assumed to run on battery and have a mesh structure, compared to a tree typically used in IAB systems. This makes the problem mostly akin to keeping the network on as long as possible and routing more flexible. On the other hand, IAB networks typically have access to a stable power source, and the main concern with energy efficiency is to reduce the economic cost and carbon footprint of the network. These differences give rise to significantly diverging problems.

Finally beyond IAB networks, the problem of tackling Signal to Interference plus Noise Ratio (SINR) constraints in optimization problems is long-standing issue which our article also tackles. In some simple cases, this type of formulations can be solved through convex reformulations [25], which has been leveraged in various related contexts such as beamforming [26] and power allocation [27]. However, these approaches overlook inter dependencies between power

allocation and link capacity, and treat SINR constraints in isolation.

B. Our Contributions

In this paper, we address the challenge of designing dynamic IAB networks that aim to provide connectivity for a set of UEs meeting the service requirements and minimizing energy consumption. We study the problem of identifying a tree from the network which has IAB-donor as root, IAB-nodes as intermediate nodes, and UEs as leaves. To achieve this goal, we propose comprehensive optimization frameworks that include 3rd Generation Partnership Project (3GPP)-compliant realistic capacity modeling. To enable a practical deployment, the optimization solution that defines and controls the IAB network topology is designed to be deployed as an rApp that runs on the non-real-time RIC within the O-RAN architecture, as also shown in Fig. 1. The main contributions of this paper are as follows:

- Formulation of joint routing, resource allocation and energy minimization problem. We employ dynamic IAB node activation and power control with the goal of energy minimization, at the same time guaranteeing minimum data rate requirements.
- Formulation of joint routing, resource allocation, and power control with the objective of maximizing the minimum data rate achieved by the UEs. Unlike problems considering fixed power, joint power allocation optimization enables to achieve better throughput performance.
- Design of a novel capacity model that defines achievable link capacity by linking power levels to data rates. This is different from existing literature, where the network capacity is often simplified ignoring the dependency between power, SINR, and data rates. This helps to integrate power-dependent capacity constraints into optimization framework. We also address the challenge of incorporating SINR constraint in the optimization problem.
- Development of two practical large-scale approaches to solve the energy optimization and throughput maximization problems. One of the approaches employs an iterative search strategy that refines solutions, while the other simplifies the optimization process by reducing the problem size.

- Evaluation over different real-world scenarios, based on a real network dataset, to demonstrate the effectiveness of the proposed approaches.

Our detailed analysis of the proposed solutions over realistic scenarios shows their distinct performance characteristics and trade-offs. This enables the network operators to make informed method selections according to the deployment and performance requirements and frequency band characteristics.

The rest of the paper is organized as follows. In Sec. II, we discuss the system model in detail, including the energy, channel, and capacity models. We formulate the optimization problems in Sec. III. Sec. IV presents the heuristic solutions for the problems. In Sec. V, we discuss the evaluation set up, followed by discussion of performance evaluation in Sec. VI. Finally, in Sec. VII, we conclude the paper.

II. SYSTEM MODEL

A. IAB Architecture

We consider a downlink transmission scenario in an IAB network with IAB-nodes assisting the IAB-donor to provide service to a set of UEs. Each IAB-node is divided into two main parts: the baseband processing unit, which includes both the DU and the MT, and the radio frontend, which enables both the DU and the MT to communicate with other IAB nodes or UEs. In order to support spatial diversity, the RF frontend is divided into up to three distinct sectors, which can be activated on demand. The IAB-donor is connected to the core network with a wired (fiber) backhaul and has a Central Unit (CU), a DU connected to the CU, and the RF frontend, also divided into three distinct sectors. An example of IAB network is presented in Fig. 1.

Let us now introduce the problem formally. We start from a weighted directed graph $\mathcal{G} = (\mathcal{V}, \mathcal{E})$, called measurements graph, constructed from UE measurement reports. The network topology consists of UEs, IAB-nodes, and IAB-donor. For detailed and more accurate graph representation, we split an IAB-node to its MT+DU unit and individual RF front end units corresponding to each sector (we assume that each of the MT+DU unit are interconnected to the RF front end via a wired link, see Fig. 1). As frontends serve different sectors with different transmission capabilities, this decomposition enables to optimize power and resource allocation individually. Then, the vertices of the graph include:

- UEs, denoted as $\mathcal{U} \subset \mathcal{V}$, which need to connect to the network in order to receive downlink traffic;
- IAB frontend radios, denoted as $\mathcal{R} \subset \mathcal{V}$, where each node corresponds to a RF frontend in an IAB-node;
- MT+DU units, denoted as $\mathcal{M} \subset \mathcal{V}$. Each unit is connected to one or several RF frontends.

We denote by $\mathcal{W} \subset \mathcal{E}$ the set of wireless links, which are weighted by their pathloss, and by $\mathcal{F} \subset \mathcal{E}$ the internal connections which connect MT+DU unit to their respective RF frontends. Since the goal is to find a tree representing the routing from the donor towards each UE, the edges of the graph will be directed accordingly. Access links are always directed from IAB frontend radio to UEs, with the IAB frontend radio as the source and the UE as the destination. Backhaul links from other IAB-nodes or IAB-donor are always directed towards the MT+DU unit.

Each IAB-node maintains information about UEs and the potential wireless links through measurements reports. The O-RAN architecture allows extensions to standard interfaces so that we can assume that the local information can be collected by an rApp, running on the non-real-time RIC, which reconstructs the measurements graph we mentioned above. Then, the optimization algorithm periodically runs and pushes the optimized topology to the RAN through the O1 interface (we discuss extensions of the O-RAN architecture to enable IAB in [9]). Note that we take into consideration periodic updates of the topology with a period in the order of minutes, so we assume that disabled nodes wake up to receive an updated topology with a similar schedule. This schedule is also perfectly compatible with the non-real-time RIC closed-loop time constraints. Without loss of generality in the following model we will assume the optimization of a single tree, but the proposed optimization model can be trivially adapted to optimize multiple trees.

B. Energy Model

1) *Power consumption as a function of transmission power:* We adopt the EARTH model [28] to model energy consumed by RF frontends formulated as:

$$P_{in} = \begin{cases} N_{TRX} \times P_0 + \Delta_p P_{tx}, & 0 < P_{tx} \leq P_{max} \\ N_{TRX} \times P_{sleep} & P_{tx} = 0 \end{cases} \quad (1)$$

where N_{TRX} is the number of RF transmission chains per frontend, P_0 is the power consumed when the RF frontend is not transmitting, Δ_p is the rate of increase of the power consumption given the current transmission power P_{tx} , and P_{max} is the maximum transmission power. $N_{TRX}, P_0, \Delta_p, P_{max}$ are constant parameters which depend on the RF frontend configuration, hence this model is linear. Even if a node is not actively used in the topology, we assume it is in sleep mode, consuming a minimal amount of power P_{sleep} . Also, it wakes up periodically to check for potential inclusion in the updated IAB topology.

2) *Scheduling Considerations:* Our model incorporates scheduling decisions to manage resources. Since the whole network operates using the same spectrum (*i.e.*, in-band IAB), we use Time Division Multiple Access (TDMA) scheduler that allocates radio resources to each radio link. This means we could obtain solutions where the radio is not transmitting for significant portions of the time. In those moments where the radio is not transmitting, our model deactivates the power amplifier of the associated RF frontend to save energy [29]. Hence, we derive our energy model from the EARTH model as:

$$P_{in} = \begin{cases} N_{TRX} \times P_0 + \alpha \times \Delta_p P_{tx}, & 0 < P_{tx} \leq P_{max} \\ N_{TRX} \times P_{sleep} & P_{tx} = 0 \end{cases} \quad (2)$$

where α is a number between 0 and 1 which indicates the proportion of the time when the radio is transmitting.

C. Channel Model

Let us now introduce our channel model. We assume that each IAB-node or IAB-donor obtains the receiving power at other IAB-nodes and UEs through Reference Signal Received Power (RSRP) measurement reports. In our simulations and model, the RSRP follows

the 3GPP UMi [30] channel, combined with ray tracing to evaluate whether UEs and nodes are Line of Sight (LoS) or not. Indoor UEs are considered always Non-LoS (NLoS) and we add an indoor-to-outdoor loss. Since the buildings are concrete, we use the O2I-high loss [30].

D. Capacity Model

We design a capacity model with the goal to derive a function that defines the achievable link capacity, given a set of 5G gNBs and UEs, and the respective power levels. This can be calculated using the 3GPP standard formula defined in [31] that considers Modulation and Coding Scheme (MCS), available physical resource blocks, and MIMO layers which is as follows:

$$C = 10^{-6} \sum_{j=1}^J \frac{Q_{j,m} \cdot f_j \cdot v_j \cdot C_{max} \cdot N_{B(j),\mu} \cdot 12}{T_{s,\mu}} \cdot (1 - OH_j). \quad (3)$$

Here, $Q_{j,m}$ is the modulation order, J is the number of component carriers aggregated in a band, f_j is the scaling factor reported by UE Capability information that is used to reflect maximum number of layers and modulation order with the band combination, v_j is the number of MIMO layers, $N_{B(j),\mu}$ is the number of Physical Resource Blocks (PRBs) allocated in bandwidth $B(j)$ for numerology μ , $T_{s,\mu}$ is the average symbol duration that depends on numerology, OH_j is the overhead factor.

Since this formula gives us the capacity of the link given the MCS (the other parameters are assumed fixed for each gNB), we leverage the table from 3GPP that associates SINR thresholds with MCS values to establish the relationship. The SINR of the radio link between u and v is defined as:

$$SINR(u,v) = 10 \cdot \log_{10} \frac{S_{u,v}}{I_{u,v}} \quad (4)$$

With

$$S_{u,v} = P_{tx}^u \cdot 10^{G_{tx}^u/10} \cdot 10^{G_{rx}^v/10} \cdot 10^{PL_{u,v}/10} \quad (5)$$

$$I_{u,v} = \sum_{r \in \mathcal{R} \setminus \{u,v\}} P_{tx}^r \cdot 10^{G_{tx}^r/10} \cdot 10^{G_{rx}^r/10} \cdot 10^{PL_{r,v}/10}, \quad (6)$$

where P_{tx}^i is the power of node i in mW, G_{tx}^i its transmission gain (in dBm), G_{rx}^i its reception gain (in dBm) and $PL_{i,j}$ is the pathloss (in dBm) between i and j . This enables us to link power levels and capacity as it creates a direct relationship through sequential mapping of power level, SINR, MCS and capacity.

We show an example of such a capacity function computed using the real OpenAirInterface (OAI) values in Fig. 2. Figure 2 suggests that the capacity function can be approximated by a simple model such as a piecewise-linear function of SINR. However, the problem still cannot be solved by a linear solver since the SINR is a ratio of power variables and thus introduces non-linearity.

Instead, we resort to analyzing the capacity as a bivariate function of the signal and of the interference. Let us now denote the capacity function as $C(S,I)$. Observe that $C(S,I)$ is a piecewise-constant function, and it is increasing with the ratio S/I . Let us note the ordered possible values of $C(S,I)$ as C_0, C_1, \dots, C_{27} where each C_i corresponds to a specific MCS. Since $C(S,I)$ is an increasing function of S/I , each capacity C_i is associated with a threshold th_i ,

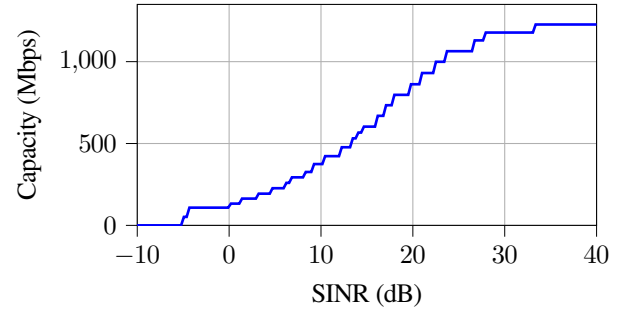


Fig. 2: Capacity as a function the SINR for link with 100 MHz bandwidth with 4 MIMO layers.

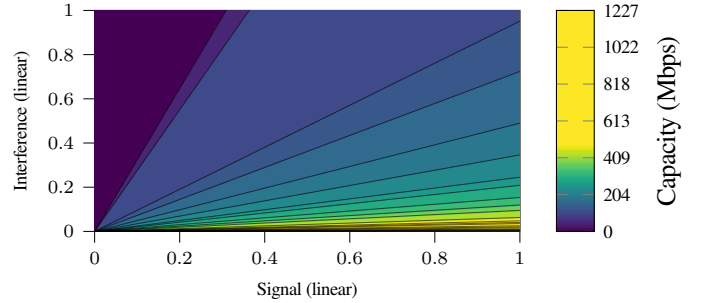


Fig. 3: Capacity Function for 100 MHz link with 4 MIMO layers.

such that $S/I \geq th_i$ ensures the link has a capacity of at least C_i . This means we have:

$$C(S,I) \geq C_i \Leftrightarrow S \geq th_i \cdot I. \quad (7)$$

This is illustrated in Figure 3, where we plot $C(S,I)$. We can observe that each of the steps of this function is defined by two lines crossing at the point such that $S = I = 0$, these lines correspond to thresholds th_{i-1} and th_i .

III. OPTIMIZATION PROBLEMS

In this section, we present two IAB topology design problem formulations: one aimed at maximizing throughput and the other at minimizing energy consumption. Our optimization models identify a tree, denoted as \mathcal{T} , which is a subgraph of \mathcal{G} , rooted in the IAB-donor, and whose leaves are the UEs. The variables and notations used in this section is summarized in Tab. I.

The TDMA scheduler operates using a weighted round-robin policy to schedule the inbound traffic and a dedicated radio device to relay the outbound traffic. This additional constraint—which follows guidance from 3GPP technical documents [32]—differentiates our model from a classical multicommodity flow problem, where adjacent edges do not have to share the same time resources as in a wireless network.

We formulate the problem as a mixed integer multicommodity flow problem. In such a problem, we have to route a set of \mathcal{K} commodities on the graph, each using a single path. A commodity $k \in \mathcal{K}$ is defined as a tuple s_k, t_k where s_k is the source node (in our case, the IAB-donor t) and t_k is the destination node (in our case,

TABLE I: System Variables and Notation

Graph Structure	
$\mathcal{G} = (\mathcal{V}, \mathcal{E})$	Weighted directed measurements graph
$\mathcal{U} \subset \mathcal{V}$	Set of user equipment (UEs)
$\mathcal{R} \subset \mathcal{V}$	Set of IAB frontend radios
$t \in \mathcal{V}$	DU of the IAB-donor node
$\mathcal{W} \subset \mathcal{E}$	Set of wireless links (weighted by pathloss)
$\mathcal{F} \subset \mathcal{E}$	Set of wired links (infinite capacity)
$\mathcal{N}_{out}(v)$	Outgoing neighbors of node v
$\mathcal{N}_{in}(v)$	Incoming neighbors of node v
$\mathcal{N}_{all}(v)$	All neighbors: $\mathcal{N}_{in}(v) \cup \mathcal{N}_{out}(v)$
$out(v) \in \mathbb{Z}^+$	Outgoing degree: $ \mathcal{N}_{out}(v) $
$in(v) \in \mathbb{Z}^+$	Incoming degree: $ \mathcal{N}_{in}(v) $
$deg(v) \in \mathbb{Z}^+$	Total degree: $out(v) + in(v)$
Commodity and Routing	
\mathcal{K}	Set of commodities to be routed
$k \in \mathcal{K}$	Commodity defined as tuple (s_k, t_k)
$s_k \in \mathcal{U}$	Source node of commodity k (UE)
$t_k = t$	Destination node of commodity k (IAB-donor)
$d_k \in \mathbb{R}^+$	Traffic demand for commodity k
Flow Variables	
$f_k(u, v) \in \mathbb{R}^+$	Flow rate of commodity k on edge (u, v)
$f(u, v) \in \{0, 1\}$	Binary indicator: edge (u, v) used by any commodity
Node State Variables	
$a(u) \in \{0, 1\}$	Binary indicator: node u is turned on (1) or sleeping (0)
Power and Resource Variables	
$P_{tx}^u \in [0, P_{\max}^u]$	Transmission power of node u
P_0	Power consumed when gNB is not transmitting
P_{sleep}	Power consumption in sleep mode
Δ_p	Power consumption increase rate
$\alpha(u, v) \in [0, 1]$	Time fraction allocated by node u to node v
Capacity and Quality Variables	
$\phi_i(u, v) \in \{0, 1\}$	Binary: SINR condition in Eq. (7) satisfied
$c(u, v) \geq 0$	Link capacity of edge (u, v)

a UE). Additionally, a demand $d_k \in \mathbb{R}$ can be defined as the amount of traffic to route between s_k to t_k . These commodities are decided by the Mobile Network Operator (MNO) beforehand, depending on the minimum capacity it wants to guarantee to its customers, and might be differentiated by different classes. The MNO can feed this information to the rApp running the optimization problem.

The information about each IAB node is also available and can be fed to the rApp: we denote by $G_{tx}^u + G_{rx}^u$ the transmission and reception gain of each node. Furthermore, we assume that it is possible to measure the pathloss $PL^{u,v}$ between nodes u and v .

We denote by $\mathcal{N}_{out}(v)$ the outer neighbors of node v and by $\mathcal{N}_{in}(v)$ its inner neighbors. We also have $\mathcal{N}_{all}(v) = \mathcal{N}_{in}(v) \cup \mathcal{N}_{out}(v)$. The cardinality of these sets (e.g., the outer and inner degrees) are denoted by $out(v)$ and $in(v)$, and their sum (the degree of the node) $deg(v) = out(v) + in(v)$.

We now introduce the flow allocation variables. $f_k(u, v)$ denote rate of data flow for commodity k that uses edge $(u, v) \in \mathcal{E}$, and binary variable $f(u, v)$ indicate whether (u, v) is used by any commodity. We also introduce variable $P_{tx}(v)$ which controls the transmission power of node v , and variables $\phi_i(u, v)$ indicating whether the Signal and Interferences of edge (u, v) are such that the condition in equation (7) holds. Furthermore we introduce variable

$\alpha(u, v) \in [0, 1]$ which decides what portion of the total transmission time of node u is allocated to node v . Further, we denote the capacity of each edge $(u, v) \in \mathcal{W}$ as $c(u, v)$.

A. Throughput Maximization Problem

In this section, we present throughput maximization problem. Instead of maximizing the aggregate throughput of the entire IAB network, we maximize the minimum throughput achieved by any UE in the IAB network. The goal of formulating such an objective is to make sure to maintain consistent Quality of Service (QoS) via minimum guaranteed throughput among the UEs served. The throughput maximization problem can be formally stated as follows:

$$\max_{f, f_k, \alpha, P_{tx}} Z \quad (8)$$

Subject to:

$$\sum_{v \in \mathcal{V}} f_k(u, v) - \sum_{v \in \mathcal{V}} f_k(v, u) = 0 \quad \forall k \in \mathcal{K}, \forall u \in \mathcal{V} \setminus \{s_k, t_k\} \quad (9)$$

$$\sum_{v \in \mathcal{V}} f_k(s_k, v) - \sum_{v \in \mathcal{V}} f_k(v, s_k) = -(\sum_{v \in \mathcal{V}} f_k(v, t_k) - \sum_{v \in \mathcal{V}} f_k(t_k, v)) \quad \forall k \in \mathcal{K} \quad (10)$$

$$\sum_{v \in \mathcal{N}_{all}(u)} \alpha(u, v) \leq 1 \quad \forall u \in \mathcal{V} \quad (11)$$

$$f(u, v) \geq \alpha(u, v) \quad \forall (u, v) \in \mathcal{E}, k \in \mathcal{K} \quad (12)$$

$$\sum_{v \in \mathcal{N}_{in}(u)} \mathbb{1}_{u \in \mathcal{R}} \cdot f(u, v) \leq 1 \quad \forall u \in \mathcal{R} \cup \mathcal{U} \quad (13)$$

$$\sum_{u \in \mathcal{N}_{in}(v)} f_k(u, v) \geq Z \quad \forall v \in \mathcal{U} \quad (14)$$

$$\sum_{k \in \mathcal{K}} f_k(u, v) \leq c(u, v) \quad \forall (u, v) \in \mathcal{W} \quad (15)$$

$$\phi_i(u, v) = 1 \implies \{S_{u,v} \geq th_i(u, v) \times I_{u,v}\} \quad \forall i \in [0, 27], \forall (u, v) \in \mathcal{W} \quad (16)$$

$$\phi_i(u, v) = 0 \implies \{S_{u,v} \leq th_i(u, v) \times I_{u,v}\} \quad \forall i \in [0, 27], \forall (u, v) \in \mathcal{W} \quad (17)$$

$$c(u, v) \leq (\phi_i(u, v) * C_i(u, v) + (1 - \phi_i(u, v)) * C_{27}(u, v)) \cdot \alpha(u, v) \quad \forall i \in [0, 27], \forall (u, v) \in \mathcal{W} \quad (18)$$

(5)

(6)

$$\phi_i(u, v) \in \{0, 1\} \quad \forall i \in [0, 27], \forall (u, v) \in \mathcal{W} \quad (19)$$

$$P_{tx}^u \in [0, P_{\max}^u] \quad \forall u \in \mathcal{R} \quad (20)$$

$$f(u, v) \in \{0, 1\} \quad \forall (u, v) \in \mathcal{E} \quad (21)$$

$$\alpha(u, v) \in [0, 1] \quad \forall (u, v) \in \mathcal{E} \quad (22)$$

$$f_k(u, v) \in \mathbb{R}^+ \quad \forall (u, v) \in \mathcal{E}, \forall k \in \mathcal{K} \quad (23)$$

$$Z \in \mathbb{R}^+ \quad (24)$$

The objective, Z is bounded by the smallest throughput received by all UEs due to constraint (14). In this formulation, we do not impose d_k , the demand requirement of commodity k . We note that

the objective function (8) combined with constraint (14) is equivalent to the following max-min objective:

$$\max_{\mathbf{f}, \mathbf{f}_k, \alpha, P_{tx}} \min_{v \in \mathcal{U}} \left\{ \sum_{u \in \mathcal{N}_{in}(v)} f_k(u, v) \right\}. \quad (25)$$

Constraints (9) and (10) are flow conservation constraints. Constraint (11) ensures that we do not schedule more time resources than possible, constraint (32) ensure that link variables are equal to 1 if the link carries some flow, (13) prevents UEs and RF frontends from having more than 1 inner neighbor, which forces the topology to be a tree. Constraint (15) defines the maximum capacity of the wireless links. The expression of the capacity $c(u, v)$ is calculated according to the description of Section II-D: we have one binary variable $\phi_i(u, v)$ per capacity value of each wireless link (u, v) . Then, the indicator constraints (16) and (17) ensure that this variable is equal to 1 if the link (u, v) can achieve the i^{th} capacity level C_i and zero otherwise. Such implication constraints are standard in modern solvers which transform them into mixed binary formulations efficiently [33]. Then, in constraint (18), we ensure that the capacity of the link (u, v) respects the capacity values given by the thresholds. Note that this value given by the thresholds is multiplied by the scheduling variable of the link $\alpha(u, v)$. This gives a non-linear constraint. However, since the non-linearity comes from the product of a binary and a continuous variable, modern solvers such as Gurobi, CPLEX or OR-Tools can linearize this equation.

B. Energy Minimization Problem

We now introduce the variant of the same problem which optimizes for energy consumption minimization. Let us introduce the binary variables $a(v) \forall v \in \mathcal{V}$ which indicate whether node v is turned on or sleeping. As discussed in the previous section, nodes consume a minimal amount of power P_{sleep} when it is turned off. Then using Eq. (2), the aggregate power consumption across the entire IAB network can be represented as:

$$P_{total} = \sum_{v \in \mathcal{V}} (1 - a(v)) \times P_{sleep} + \sum_{v \in \mathcal{V}} a(v) \times P_0 + \sum_{u \in \mathcal{V}} \sum_{v \in \mathcal{N}_{out}(u)} a(v) \times P_{tx}^u \times \alpha(u, v) \times \Delta_P. \quad (26)$$

The first part of the function is the static baseline power consumption of a RF frontend. It is either P_{sleep} if the RF frontend is not activated or P_0 if it is activated.

Based on this, the energy minimization problem can be formally stated as follows:

$$\min_{\mathbf{f}, \mathbf{f}_k, \alpha, P_{tx}, \mathbf{a}} P_{total} \quad (27)$$

Subject to:

$$\sum_{v \in \mathcal{V}} f_k(u, v) - \sum_{v \in \mathcal{V}} f_k(v, u) = 0 \quad \forall u \in \mathcal{V}, \forall k \in \mathcal{K} \quad (28)$$

$$\sum_{v \in \mathcal{V}} f_k(s_k, v) - \sum_{v \in \mathcal{V}} f_k(v, s_k) = 1 \quad \forall k \in \mathcal{K} \quad (29)$$

$$\sum_{v \in \mathcal{V}} f_k(v, t_k) - \sum_{v \in \mathcal{V}} f_k(t_k, v) = -1 \quad \forall k \in \mathcal{K} \quad (30)$$

$$\sum_{k \in \mathcal{K}} f_k(u, v) \cdot d_k \leq c(u, v) \quad \forall (u, v) \in \mathcal{W} \quad (31)$$

$$f(u, v) \geq f_k(u, v) \quad \forall (u, v) \in \mathcal{E}, k \in \mathcal{K} \quad (32)$$

$$(5), (6), (11), (32), (13), (16), (17), (18), (19), (20), (21), (22)$$

$$f_k(u, v) \in \{0, 1\} \quad \forall (u, v) \in \mathcal{E}, \forall k \in \mathcal{K} \quad (33)$$

$$a(v) \in \{0, 1\} \quad \forall v \in \mathcal{V} - \mathcal{U} \quad (34)$$

Equation (27) is the objective function that considers node activation. In this formulation, we consider the demand d_k for each commodity k . Thus the variables $f_k(u, v)$ indicate whether commodity k uses edge $(u, v) \in \mathcal{E}$ and thus are binary (instead of being continuous in the previous problem). Consequentially, the flow conservation constraints change (equations (28), (29) and (30)). Capacity constraints (31) now take the demand of the commodity d_k into account because the goal of the problem at hand is to route all the demands while minimizing the energy consumption. The rest of the constraints of the problem remain the same. Note that the objective function of this problem is non-convex due to the product of continuous variables $\alpha(u, v)$ and P_{tx}^u .

IV. PRACTICAL LARGE-SCALE APPROACHES

The throughput maximization and energy minimization problems generate a large search space that scales exponentially with the network size. In addition to this, non-linear relationships between variables and their tight coupling through constraints such as capacity and scheduling constraints have a significant impact on problem complexity, making it challenging to obtain exact solutions. Therefore, in this section, we discuss two algorithms designed to address the throughput maximization and energy minimization problems. The first approach employs an iterative search strategy that refines solutions such that the optimization objective is met. The crux of the second approach is problem size reduction with the goal of simplifying the optimization process and leverages pruning techniques to achieve this goal.

A. Local Search Method

The local search method is based on iterative improvements toward the optimization objective while maintaining feasibility. Instead of solving a complex global optimization problem directly, the algorithm explores different configurations locally by optimizing one frontend node $u \in \mathcal{R}$ at a time. A high-level overview of the local-search method algorithm for throughput maximization and energy minimization is provided in the Fig. 4.

The algorithm for solving the maximum throughput problem, outlined as Algorithm 1, takes measurement graph $\mathcal{G} = (\mathcal{V}, \mathcal{E})$ as input. Initially, the transmission power for all frontend nodes $u \in \mathcal{R}$ are set to their maximum values P_{max}^u . The algorithm maintains a solution vector $curr_best_sol$ that stores the best solution found so far for each node $u \in \mathcal{R}$. It also tracks the best objective value found, stored in $curr_best_obj$. The heuristic uses two phases of iterative search to converge toward a feasible optimal solution. The first phase finds an initial topology and the second phase varies power at each node to further fine-tune the solution.

In each iteration of the first phase, the algorithm follows these steps for each node: it toggles the power between 0 and P_{max}^u (lines 11-15 of Algorithm 1), fixes the power of all other nodes to the best

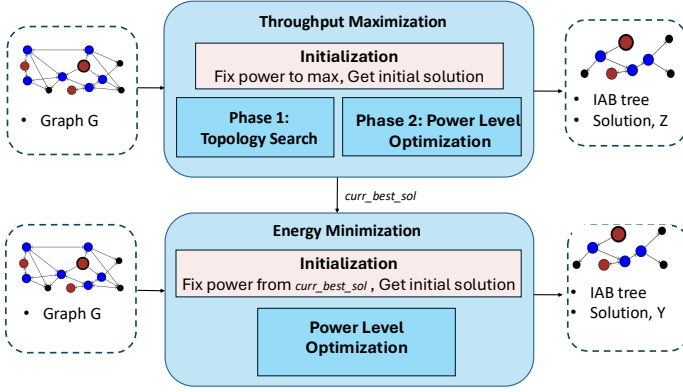


Fig. 4: Local search method.

Algorithm 1 Local search method for solving the maximum throughput problem

Input: Measurement Graph

Output: Flow Allocation with maximum throughput

```

1: Fix all power variables  $P_{tx}^u$  to  $P_{max}^u \forall u \in \mathcal{R}$ 
2: Solve (8) - (24) and obtain objective value  $Z$ 
3:  $curr\_best\_obj = Z$ 
4:  $prev\_best\_obj = -1$ 
5:  $curr\_best\_sol = Dict()$ 
6: for  $u \in \mathcal{R}$  do
7:    $curr\_best\_sol[u] = P_{max}^u$ 
8:   while  $curr\_best\_obj \neq prev\_best\_obj$  do
9:      $prev\_best\_obj = curr\_best\_obj$ 
10:    for  $u \in \mathcal{R}$  do
11:      if  $curr\_best\_sol[u] == 0$  then
12:         $val = P_{max}^u$ 
13:      else
14:         $val = 0$ 
15:      fix value of  $P_{tx}^u$  to  $val$ 
16:      fix value of  $P_{tx}^v$  to  $curr\_best\_sol[v] \forall v \in \mathcal{R} - \{u\}$ 
17:      Solve optimization problem (8) - (24), obtain objective value  $Z$ 
18:      if  $Z \geq curr\_best\_obj$  then
19:         $curr\_best\_sol[u] = val$ 
20:         $curr\_best\_obj = Z$ 
21:    while  $curr\_best\_obj \neq prev\_best\_obj$  do
22:       $prev\_best\_obj = curr\_best\_obj$ 
23:      for  $u \in \mathcal{R}$  do
24:        unfix  $P_{tx}^u$  if it was fixed
25:        fix value of  $P_{tx}^v$  to  $curr\_best\_sol[v] \forall v \in \mathcal{R} - \{u\}$ 
26:        Solve (8) - (24) and obtain objective  $Z$ 
27:        if  $Z > curr\_best\_obj$  then
28:           $curr\_best\_sol[u] = P_{tx}^u$ 
29:           $curr\_best\_obj = Z$ 
30: return Solution obtained by solving (8) - (24) with  $P_{tx}^u$  fixed to  $curr\_best\_sol[u] \forall u \in \mathcal{R}$ .

```

Algorithm 2 Local search method for solving the minimum energy problem

Input: Measurement Graph

Output: Flow Allocation with minimum energy

```

1: Obtain a maximum throughput solution via Algorithm 1.
2: for  $u \in \mathcal{R}$  do
3:    $curr\_best\_sol[u] = P_{tx}^u$ 
4:   for all  $k \in \mathcal{K}$  do
5:     if  $d_k \geq Z$  then
6:       return "failed to find a feasible solution"
7:   fix value of  $P_{tx}^u$  to  $curr\_best\_sol[u] \forall u \in \mathcal{R}$ 
8:   Solve (27) - (34) and obtain energy consumption value  $Y$ .
9:    $curr\_best\_obj = Y$ 
10:   $prev\_best\_obj = -1$ 
11:  while  $curr\_best\_obj \neq prev\_best\_obj$  do
12:     $prev\_best\_obj = curr\_best\_obj$ 
13:    for  $u \in \mathcal{R}$  do
14:      unfix  $P_{tx}^u$  if it was fixed
15:      fix value of  $P_{tx}^v$  to  $curr\_best\_sol[v] \forall v \in \mathcal{R} - \{u\}$ 
16:      Solve (27) - (34) and obtain objective  $Y$ 
17:      if  $Y > curr\_best\_obj$  then
18:         $curr\_best\_sol[u] = P_{tx}^u$ 
19:         $curr\_best\_obj = Y$ 
20: return Solution obtained by solving (27) - (34) with  $P_{tx}^u$  fixed to  $curr\_best\_sol[u] \forall u \in \mathcal{R}$ .

```

solution found so far (line 16 of Algorithm 1), solves the optimization problem (line 17 of Algorithm 1), and checks if this leads to a higher throughput Z . If a higher throughput is found, it updates the solution and objective variables, $curr_best_sol$ and $curr_best_obj$, for the corresponding node (lines 18-20 of Algorithm 1). Subsequently, the first phase results in an initial IAB network topology.

The second phase further refines the solution space by following these steps: it fixes transmission power of all nodes except one at a time using the best solution found so far from $curr_best_sol$ (lines 24-25 of Algorithm 1). Then it solves the optimization problem (line 26 of Algorithm 1). Similar to the previous phase, the solution is checked for convergence followed by updating the best solution (lines 28-29 of Algorithm 1). This process is repeated until no further improvements in throughput can be made and the algorithm returns the final solution.

The algorithm for solving energy minimization problem is outlined as Algorithm 2. First, it obtains the maximum throughput solution using Algorithm 1. Then it checks if the demand constraints are met for all the commodities by $d_k \geq Z \forall k \in \mathcal{K}$. The algorithm then fixes the power values from the solution of throughput maximization, obtained as $curr_best_sol$, and solves the energy minimization problem (lines 7-8 of Algorithm 2). Similar to the second phase of Algorithm 1, the solution is iteratively refined by fixing transmission power of all nodes except one at a time using the best solution from the solution vector $curr_best_sol$ and solving the optimization problem (lines 12-19 of Algorithm 2). This is repeated until convergence and the algorithm returns the solution.

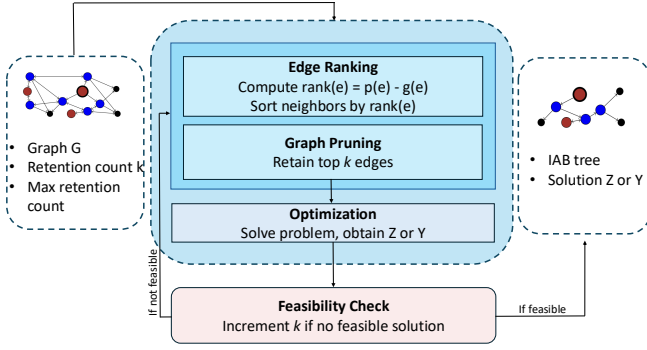


Fig. 5: Selective-reduction method.

B. Selective-Reduction Method

The selective-reduction method simplifies the original problem by preserving only a subset of edges from the IAB network and eliminating those that are least likely to appear in the optimal subset. This reduces the problem size and consequently makes it easier to solve.

An overview of the approach is provided in Fig. 5 and algorithm is outlined as Algorithm 3. We note that the method can be leveraged for solving either of the two optimization problems.

Algorithm 3 Selective-reduction method

Input: Measurement Graph G , Initial Retention Count (k), Maximum Retention Count (max_ret_count)

Output: Flow Allocation with Maximum Throughput

- 1: Set $feasible_solution = \text{false}$
 - 2: **while** $k \leq max_ret_count$ **do**
 - 3: Compute $rank$ for each edge $e \in \mathcal{W}$ as $g(e) - p(e)$ {Gain minus pathloss}
 - 4: Sort $N(u)$ in descending order of $rank$
 - 5: Retain the top k edges from $N(u)$ and add them to E'
 - 6: Solve optimization problem (8) - (24), obtain objective value Z or solve (27) - (34), obtain objective value Y
 - 7: **if** Z or Y is feasible **then**
 - 8: Store solution and set $feasible_solution = \text{true}$
 - 9: **break**
 - 10: **else**
 - 11: Increase k
 - 12: **return** solution with objective Z or Y
-

One of the key aspects in pruning-based approaches is to determine an effective pruning strategy. Another is to ensure that the pruning process is not aggressive and that the pruning process does not cause solution infeasibility. We address these as follows:

- **Edge ranking:** We weight the edges using an appropriate metric and rank these weighted edges as a first step in the pruning process.
- **Retention count parameter:** This variable controls the pruning intensity by specifying the number of neighbors to retain during the pruning process.
- **Adaptive Fine-Tuning:** The retention count is incremented until a feasible solution is achieved and this ensures that the pruning process is not aggressive.

	Scenario 1	Scenario 2
Area [km ²]	0.092	0.132
UE density [UE/km ²]	0–900	0–900
Path Loss Model	3GPP 38.901	
Frequency [GHz]	3.6, 7	
gNB Lobes gain (Main/Side) [dBi]	24/–2	
UE Main lobe gain (Main/Side) [dBi]	0/–17.85	
gNB Type	Micro-cell (see [28])	
Max tx power [W]	6.3	

TABLE II: Parameters for the simulation

The selective-reduction method given in Algorithm 3 takes measurement graph $\mathcal{G} = (\mathcal{V}, \mathcal{E})$ as input along with the initial retention count and maximum retention count. We rank each wireless link $e \in \mathcal{W} \subset \mathcal{E}$ using the metric $g(e) - p(e)$ where $g(e)$ is the gain of the link e and $p(e)$ is the pathloss of link e . While pathloss gives an indication of distance and is often used as a pruning metric (e.g., [34]), we use gain-pathloss metric as it provides a representation of effective link quality when pruning edges in the network. The edges ranked by the metric are then sorted in descending order. For each node, all the neighboring edges other than top k edges are removed from the graph. After this process, the graph with reduced size is used to solve the optimization problem. Algorithm returns the solution along with the corresponding objective value if it is found. If no feasible solution is found, the algorithm increments retention count and the whole process is repeated to check for a feasible solution.

V. PERFORMANCE EVALUATION SETUP

We evaluate our approaches using publicly available traffic data from Milan, Italy, which include two months of network operator measurements [35]. We select two representative areas for evaluation from this dataset: a highly dynamic urban area surrounding a major train station and an area of 0.092 km² in the center of Milan.

We now discuss the techniques used to synthetically generate the set of measurement graphs $\mathcal{G} = (\mathcal{V}, \mathcal{E})$, needed to evaluate the feasibility and effectiveness of our optimization model. We employ the same techniques that we use in our previous work for IAB-node placement and data-driven time-varying UE density model [7]. However, for completeness, we describe both of them in this paper.

The parameter values that we use for the simulations are presented in Table. II. Apart from the frequency bands FR1 and FR2 of 5G-NR, the upper mid-band with frequency range spanning from 7 GHz to 24 GHz, also known as FR3, was introduced in 3GPP Release 16 and has emerged as a focus of interest in 6G networks [36], [37]. We analyze the results with an IAB network that operates at frequencies in the frequency range FR1 and FR3. One operates at 3.6 GHz in FR1 that is commonly used with bandwidth of 100 MHz. The other operates at 7 GHz, in FR3, with higher capacity (bandwidth of 400 MHz).

A. Placement of gNBs and UEs

The set of nodes of our graph \mathcal{V} is comprised of both IAB-nodes, and UEs, whose placement is done separately using two different techniques. IAB-nodes are placed on building facades with a given density λ_{gNB} . The exact position is computed by using a state-of-the-art placement heuristic [38] that leverages highly precise

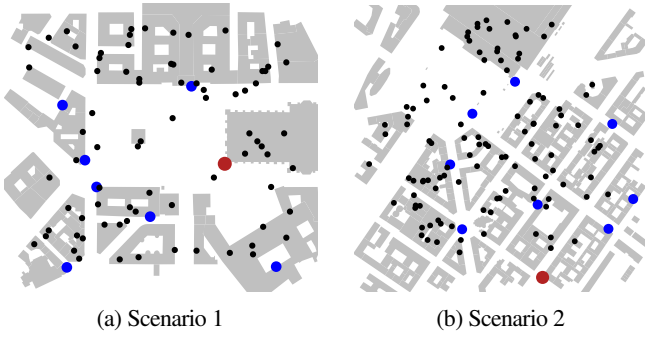


Fig. 6: Sample deployment of a network in center of Milan and train station.

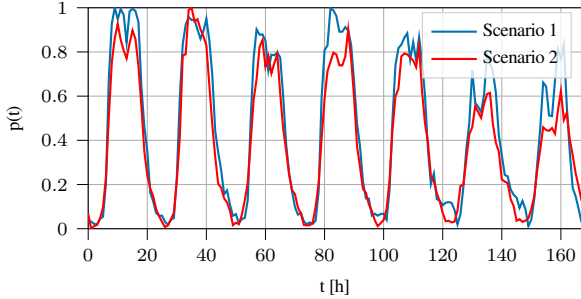


Fig. 7: Weekly normalized cell load profile of the two scenarios.

3D models to place the gNB such that the number of potential UE location in line of sight is maximized. UEs are then randomly distributed both in public areas, such as streets, and inside buildings. Specifically, given a density of λ_{UE} , indoor UEs are uniformly randomly distributed inside buildings with a density equal to $r_{i/o} \lambda_{UE}$ and outdoor UEs are uniformly distributed inside buildings with density $(1 - r_{i/o}) \lambda_{UE}$. $r_{i/o}$ is a commonly used ratio of indoor to outdoor UE, which we set to 0.8 based on 3GPP technical report [39]. In short, we consider that in our simulations, 80% of the UEs are placed indoors. Figure 6 shows sample deployment of the network in the center of Milan and train station respectively.

B. Time-varying UE Density Model

Most studies dealing with topology optimization focus their analysis on a single, or a handful, value of λ_{UE} . Since the energy optimization technique we devise tunes the IAB-node activation on the basis of the number of UEs and their load, we need to evaluate our model on a varying values of UE density, ideally following a realistic trend. Therefore, we employ a technique used in similar research [40] to devise a time-varying UE density. First, we extract the cell load profile $p(t)$ related of each area from openly available datasets [35]. This is then normalized in the range $(0,1]$. We model UE density as $\lambda_{UE}(t) = p(t)l\lambda_{gNB}$, a function of time, where $l=10$ is the number of UEs per gNBs taken from 3GPP technical report [39]. Finally, based on this model, we generate a set of 168 graphs—one for each hour of the week—capturing the temporal variation at one-hour granularity. The hourly trend of $\lambda_{UE}(t)$ corresponding to the two areas of analysis are shown in Fig. 7.

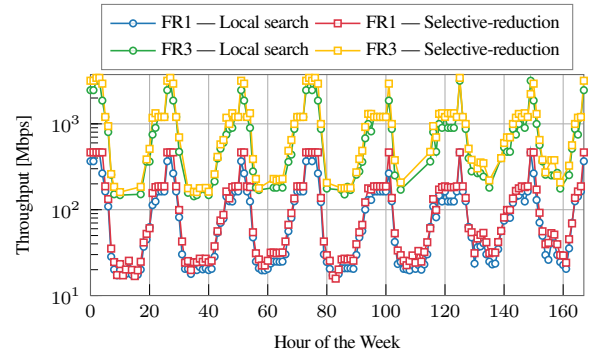


Fig. 8: Throughput performance of two approaches in scenario 1.

VI. RESULTS

In this section, we discuss the results of our approaches in detail. We compare the results for both scenarios detailed in the previous section. The measurement graphs are generated for each hour of the week, totaling 168 hours and we run the algorithms on these.

In the first part of the section, we compare the throughput obtained for local search and selective-reduction approaches. Then, in the second part, we evaluate the energy consumption in terms of power, number of nodes activated and energy efficiency for both strategies.

A. Results on Throughput Maximization

To analyze the throughput achieved by the IAB networks, we first show the hourly throughput measured over a week for scenario 1 using local search and selective-reduction approaches, which is presented in Fig. 8. We note that in the evaluations, initial retention count and maximum retention count for the selective-reduction method are set as 5 and 10 respectively.

The periodic fluctuation in the throughput achieved can be attributed to the varying user density corresponding to the peak and non-peak hours of a day. We observe that the selective-reduction method provides slightly higher throughput than the local search method and we note that the result is consistent across both FR1 and FR3. This improved performance is a consequence of the ranking and pruning of the links in the selective-reduction method based on effective link quality. Prioritizing link quality enables the optimization solvers to establish routes that maximize data transmission efficiency. We also present the Cumulative Distribution Function (CDF) for throughput across all evaluated scenarios in Fig. 9. The plot highlights that the selective-reduction method outperforms the local-search method in terms of throughput and maintains consistent performance across both scenarios and for both FR1 and FR3.

Fig. 10 shows the runtime required for both algorithms. We observe that the local search algorithm requires less execution time than the selective-reduction method. This advantage of the local search method stems from its problem decomposition strategy. While the selective-reduction method solves a single optimization problem with a reduced but still complex input space, the local search approach solves multiple smaller subproblems sequentially. To study the impact of network load intensity on runtime, we plot the sample runtime performance of weekday and weekend from scenario 2, where the cell load is lighter than scenario 1. The results are presented in Fig. 11.

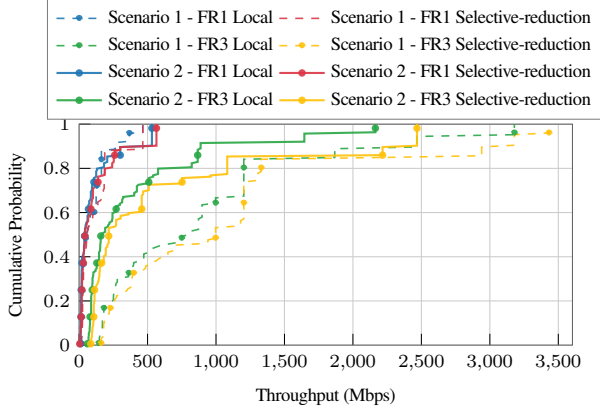


Fig. 9: Throughput CDF for both scenarios.

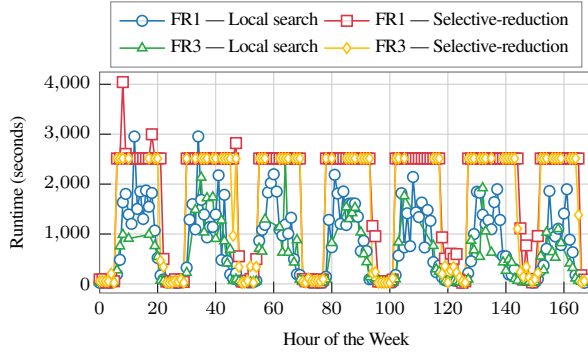
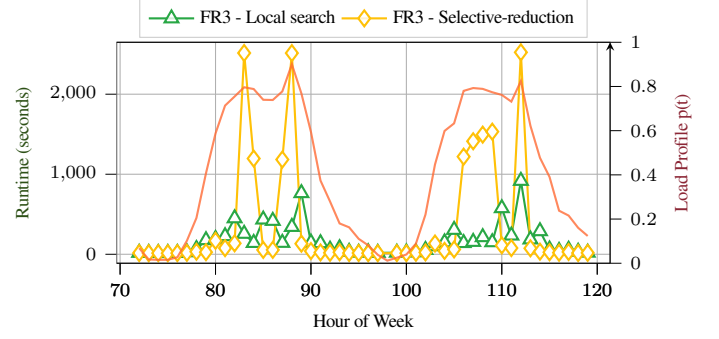


Fig. 10: Runtime performance of two approaches in scenario 1.

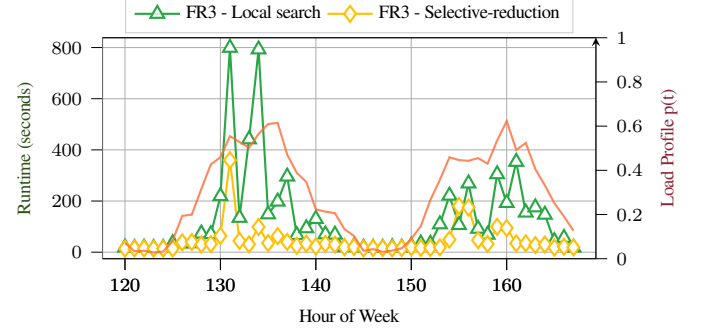
We observe that the runtime of the algorithms is heavily dependent on the network load. Selective-reduction achieves better runtime when the load is below 0.6, where the pruning effect has significant impact. This indicates the importance of fine-tuning pruning intensity by setting appropriate retention counts according to the load conditions, such as differentiating between weekend and weekdays. We note that the proposed approaches are ideal for periodic network reconfigurations on hourly timescale than real-time adaptations.

The runtime of the selective-reduction method can also be controlled explicitly by setting a limit on runtime. At the same time, runtime for local-search method is more variable and harder to control as it iteratively solves multiple simplified problems according to the convergence criteria.

As such, we analyze the evolution of the solutions over time for local-search method which provides an idea on how fast the approaches arrive at the best solution. Fig. 12 presents the convergence trajectory that shows the throughput achieved over execution time. The results are presented for one peak hour and one non-peak hour of a given day. During the peak hour, improvements in throughput are marginal despite long execution times. This highlights the importance of imposing a runtime limit in heuristic algorithms so that we can achieve trade-off on computational time and solution optimality. The solution evolution statistics for local-search method is given in Table III. The metrics captured include the initial and final throughput values, the relative improvement percentage, the time

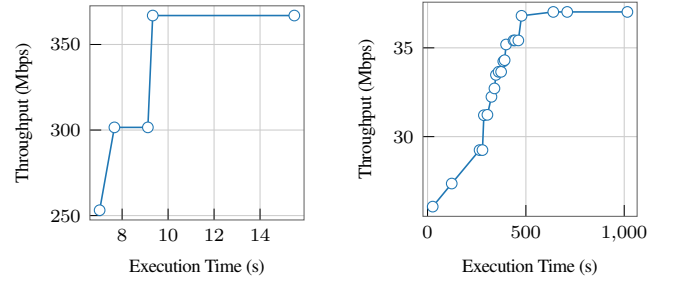


(a) Runtime performance of two weekdays day Scenario 2



(b) Runtime performance of weekend scenario 2

Fig. 11: Runtime performance- weekdays and weekend for scenario 2.



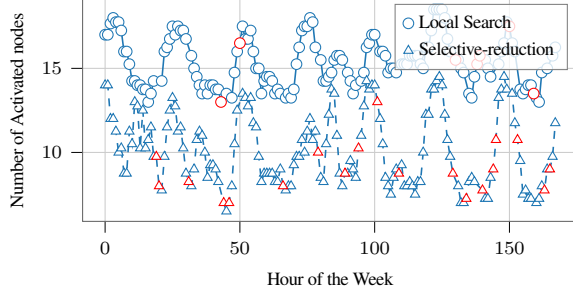
(a) Non-peak hour: Hour 0

(b) Peak hour: Hour 18

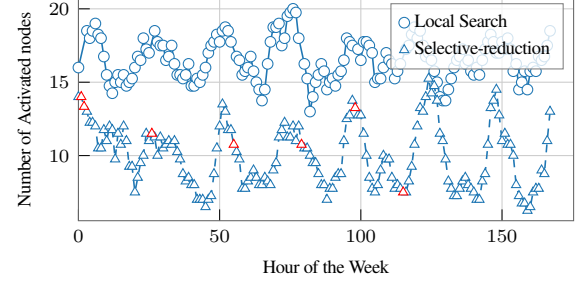
Fig. 12: Solution evolution using local search method at selected peak and non-peak hours, 3.6 GHz-100 MHz.

required to reach a near-final solution, and the total execution time.

The results reveal a distinct contrast between peak and non-peak hours. During non-peak hours, for instance, hours 0-4 or 18-21, the heuristic consistently achieves substantial improvements, with high throughput gains. Also, the algorithm converges relatively quickly. In contrast, there is little or no improvement in the solution despite extended execution times during peak hours. This implies that as the solution space becomes constrained under heavy load, time to reach an initial solution is large and the potential for the heuristic to identify significant improvements gets limited.

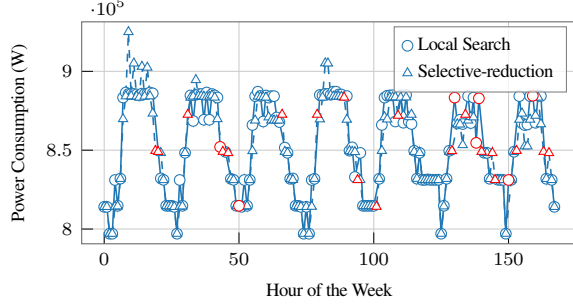


(a) RF frontend activation patterns for Scenario 1

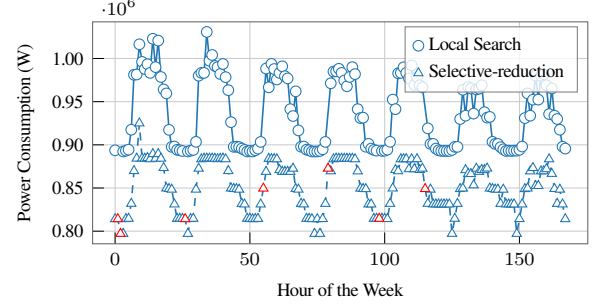


(b) RF frontend activation patterns for Scenario 2

Fig. 13: Number of activated RF frontends over a week at 3.6 GHz with 100 MHz bandwidth.



(a) Scenario 1



(b) Scenario 2

Fig. 14: Power consumption over time at 3.6 GHz with 100 MHz bandwidth.

TABLE III: Solution evolution statistics for local search method

Hour	Initial Solution	Final Solution	Improvement Percentage	Time to Near-Final	Total Execution Time
	(Mbps)	(Mbps)	(%)	(s)	(s)
0	253.14	366.91	44.95	9.33	15.49
1	253.14	366.91	44.95	8.09	14.64
2	374.46	465.27	24.25	8.01	16.80
3	374.46	465.27	24.25	7.82	15.76
4	187.23	264.59	41.32	8.12	19.92
5	163.07	163.07	0.00	—	22.03
6	98.71	109.05	10.48	25.17	130.62
7	27.69	28.33	2.31	50.78	471.13
8	20.07	20.07	0.00	26.99	494.73
9	17.19	17.19	0.00	—	27.46
10	19.77	19.80	0.14	28.82	760.64
11	17.43	17.43	0.00	27.89	1261.45
12	17.83	17.83	0.00	29.32	1312.08
13	20.45	20.45	0.00	26.38	440.68
14	17.51	17.51	0.00	—	27.05
15	17.43	17.43	0.00	26.66	1193.39
16	17.51	17.51	0.00	—	27.49
17	20.07	20.07	0.00	27.46	567.33
18	26.06	37.02	42.07	477.92	1016.11
19	41.40	44.93	8.53	193.23	1059.30
20	45.31	62.58	38.11	359.53	507.45
21	93.82	113.11	20.57	71.38	158.66
22	121.74	124.60	2.35	7.96	48.58
23	163.07	163.07	0.00	—	35.20

B. Results on Energy Minimization

To evaluate the performance in terms of energy, we analyze number of activated nodes and power consumption for different UE through-

put requirements. The minimum throughput requirement is set as 5 Mbps. The results are presented in Fig. 13 and Fig. 14 respectively. Red markers indicate hours where only one method yields a solution. From the figures, we observe that the number of activated RF frontends are fewer for the selective-reduction method compared to local-search despite higher power consumption. The result is consistent for both scenarios. This outcome is expected as selective-reduction method operates on a reduced set of connections in the IAB network.

Interestingly, we observe that the power consumption under selective-reduction method is almost similar to that of local-search method, with slight differences, especially at the peak time of the day in scenario 1. But at the same time, power consumption under selective-reduction method is much lower than that of local-search method in scenario 2. The observed variation in performance between two scenarios can be attributed to the cell-load profiles. The heavy load conditions of scenario 1, together with reduction in the edges when using selective-reduction method leads to the slightly higher power allocation. Meanwhile, under lighter load conditions, reduction in network size becomes advantageous. local search method, on the other hand, distributes power over a larger number of activated nodes, leading to higher overall power consumption.

To get more insights on the network performance-power trade-offs, we present the energy efficiency as the energy spent on transmission, defined as the ratio of achieved throughput to the total power consumption [41], [42]. This can be represented as

$$\eta(t) = \frac{B_k}{P_{total}(t)}, \quad (35)$$

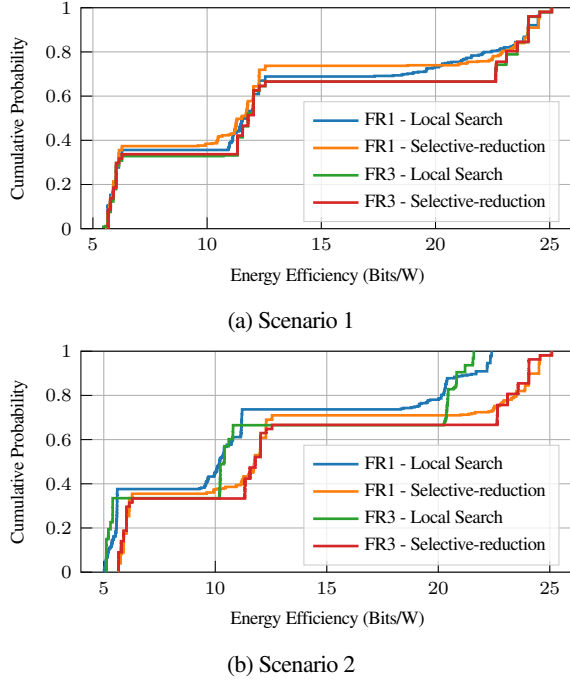


Fig. 15: Energy efficiency CDF comparison across scenarios.

where $P_{total}(t)$ is the total power required at the time period t and B_k is the throughput requirement that was guaranteed for commodity k .

Figure 15 presents the energy efficiency CDF of the algorithms under both scenarios. The CDF is computed by measuring energy efficiency across different throughput requirements to assess the consistency of algorithm performance. The energy efficiency CDF indicates that the selective-reduction method outperforms local-search method in terms of higher energy efficiency values and thus yields better throughput per unit power. The difference is quite evident in scenario 2 than in scenario 1. This result shows how well the energy is utilized by the selective-reduction method.

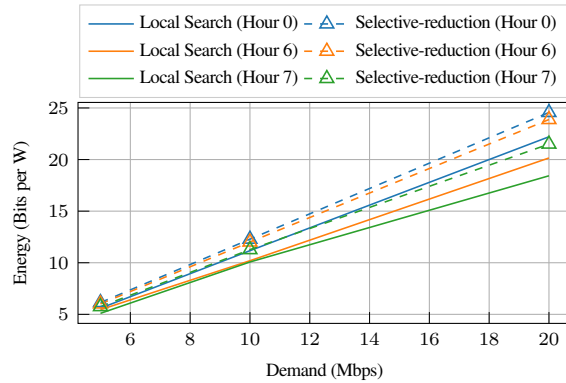


Fig. 16: Impact of data rate demand on energy efficiency (scenario 2, FR3).

We now examine the sensitivity of energy efficiency to the minimum throughput demand in peak and non-peak hours. Figure 16 presents the variation of energy efficiency with minimum throughput

requirement at 3.6 GHz. The plot shows that both algorithms become more energy efficient as minimum throughput requirements increase from 5 to 20 Mbps. This indicates that the fixed power overhead becomes less significant with higher bandwidth requirements and the power cost per additional bandwidth decreases as scale increases. At the same time, the performance gap between light and heavy load conditions widens significantly as throughput requirements increase in scenario 2. At 5 Mbps, both algorithms show minimal sensitivity to load conditions. At 20 Mbps, load sensitivity increases.

VII. CONCLUSION

In this paper, we formulated two optimization problems: a joint routing, resource allocation, and energy minimization problem, and a joint routing, resource allocation, and throughput maximization problem. To address these, we then presented two practical approaches and evaluated performance of the approaches under two realistic scenarios. Our results show that selective-reduction method achieves better energy efficiency and throughput under dynamic conditions by activating fewer nodes in the IAB network. Although the runtime of the local search method cannot be controlled like selective-reduction, the results show that it achieves better runtime under FR1 with the trade-off of throughput and number of activated nodes. This makes it a good candidate for lower frequency band deployments.

REFERENCES

- [1] S. Chen, Y.-C. Liang, S. Sun, S. Kang, W. Cheng, and M. Peng, "Vision, requirements, and technology trend of 6G: How to tackle the challenges of system coverage, capacity, user data-rate and movement speed," *IEEE Wireless Communications*, vol. 27, no. 2, pp. 218–228, 2020.
- [2] H. Lee, B. Lee, H. Yang, J. Kim, S. Kim, W. Shin, B. Shim, and H. V. Poor, "Towards 6G hyper-connectivity: Vision, challenges, and key enabling technologies," *Journal of Communications and Networks*, vol. 25, no. 3, pp. 344–354, 2023.
- [3] M. Polese, M. Giordani, T. Zugno, A. Roy, S. Goyal, D. Castor, and M. Zorzi, "Integrated access and backhaul in 5G mmWave networks: Potential and challenges," *IEEE Communications Magazine*, vol. 58, no. 3, pp. 62–68, 2020.
- [4] H. Yin, S. Roy, and L. Cao, "Routing and resource allocation for iab multi-hop network in 5G advanced," *IEEE Transactions on Communications*, vol. 70, no. 10, pp. 6704–6717, 2022.
- [5] F. I. G. Carvalho, I. B. Palhano, and T. F. Maciel, "Energy consumption analysis on integrated access and backhaul networks," in *2024 Workshop on Communication Networks and Power Systems (WCNPS)*. IEEE, 2024, pp. 1–7.
- [6] M. Feng, S. Mao, and T. Jiang, "Base station ON-OFF switching in 5G wireless networks: Approaches and challenges," *IEEE Wireless Communications*, vol. 24, no. 4, pp. 46–54, 2017.
- [7] G. Gemmi, M. Elkael, M. Polese, L. Maccari, H. Castel-Taleb, and T. Melodia, "Joint routing and energy optimization for integrated access and backhaul with open RAN," in *GLOBECOM 2023-2023 IEEE Global Communications Conference*. IEEE, 2023, pp. 1962–1967.
- [8] W. Teng, M. Sheng, X. Chu, K. Guo, J. Wen, and Z. Qiu, "Joint optimization of base station activation and user association in ultra dense networks under traffic uncertainty," *IEEE Transactions on Communications*, vol. 69, no. 9, pp. 6079–6092, 2021.
- [9] E. Moro, G. Gemmi, M. Polese, L. Maccari, A. Capone, and T. Melodia, "Toward open integrated access and backhaul with O-RAN," in *2023 21st Mediterranean Communication and Computer Networking Conference (MedComNet)*. IEEE, 2023, pp. 61–69.
- [10] M. Polese, L. Bonati, S. D'oro, S. Basagni, and T. Melodia, "Understanding O-RAN: Architecture, interfaces, algorithms, security, and research challenges," *IEEE Communications Surveys & Tutorials*, vol. 25, no. 2, pp. 1376–1411, 2023.
- [11] C. Madapatha, B. Makki, A. Muhammad, E. Dahlman, M.-S. Alouini, and T. Svensson, "On topology optimization and routing in integrated access and backhaul networks: A genetic algorithm-based approach," *IEEE Open Journal of the Communications Society*, vol. 2, pp. 2273–2291, 2021.

- [12] M. Simsek, M. Narasimha, O. Orhan, H. Nikopour, W. Mao, and S. Talwar, "Optimal topology formation and adaptation of integrated access and backhaul networks," *Frontiers in Communications and Networks*, vol. 1, p. 608088, 2021.
- [13] O. T. Ajayi, S. Zhang, and Y. Cheng, "Machine learning assisted capacity optimization for B5G/6G integrated access and backhaul networks," in *IEEE INFOCOM 2023-IEEE Conference on Computer Communications Workshops (INFOCOM WKSHPS)*. IEEE, 2023, pp. 1–6.
- [14] A. Ouerou, P. Mahey, and J.-P. Vial, "A survey of algorithms for convex multicommodity flow problems," *Management science*, vol. 46, no. 1, pp. 126–147, 2000.
- [15] O. Orhan, V. N. Swamy, T. Tetzlaff, M. Nassar, H. Nikopour, and S. Talwar, "Connection management xapp for o-ran ric: A graph neural network and reinforcement learning approach," in *2021 20th IEEE international conference on machine learning and applications (ICMLA)*. IEEE, 2021, pp. 936–941.
- [16] A. Zappone, E. Jorswieck *et al.*, "Energy efficiency in wireless networks via fractional programming theory," *Foundations and Trends® in Communications and Information Theory*, vol. 11, no. 3–4, pp. 185–396, 2015.
- [17] C. He, G. Y. Li, F.-C. Zheng, and X. You, "Energy-efficient resource allocation in OFDM systems with distributed antennas," *IEEE Transactions on Vehicular Technology*, vol. 63, no. 3, pp. 1223–1231, 2013.
- [18] F. Salahdine, J. Opadere, Q. Liu, T. Han, N. Zhang, and S. Wu, "A survey on sleep mode techniques for ultra-dense networks in 5G and beyond," *Computer Networks*, vol. 201, p. 108567, 2021.
- [19] Y. S. Soh, T. Q. Quek, M. Kountouris, and H. Shin, "Energy efficient heterogeneous cellular networks," *IEEE Journal on selected areas in communications*, vol. 31, no. 5, pp. 840–850, 2013.
- [20] W. Shang and V. Friderikos, "Energy efficient optimization of in-band integrated access and backhaul heterogeneous networks," *IEEE Transactions on Vehicular Technology*, 2024.
- [21] Y. Zhang, M. A. Kishk, and M.-S. Alouini, "Freshness-aware energy efficiency optimization for integrated access and backhaul networks," *IEEE Transactions on Wireless Communications*, 2024.
- [22] A. Salhi, J. Weinmann, M. Kochhal, and L. Schwiebert, "Power efficient topologies for wireless sensor networks," in *International Conference on Parallel Processing, 2001*. IEEE, 2001, pp. 156–163.
- [23] J. A. Torkestani, "An energy-efficient topology construction algorithm for wireless sensor networks," *Computer Networks*, vol. 57, no. 7, pp. 1714–1725, 2013.
- [24] T. Rault, A. Bouabdallah, and Y. Challal, "Energy efficiency in wireless sensor networks: A top-down survey," *Computer networks*, vol. 67, pp. 104–122, 2014.
- [25] S. P. Boyd and L. Vandenberghe, *Convex optimization*. Cambridge university press, 2004.
- [26] Q. Shi, M. Razaviyayn, M. Hong, and Z.-Q. Luo, "SINR constrained beamforming for a MIMO multi-user downlink system: Algorithms and convergence analysis," *IEEE Transactions on Signal Processing*, vol. 64, no. 11, pp. 2920–2933, 2016.
- [27] W. Hao, O. Muta, H. Gacanin, and H. Furukawa, "Power allocation for massive MIMO cognitive radio networks with pilot sharing under SINR requirements of primary users," *IEEE Transactions on Vehicular Technology*, vol. 67, no. 2, pp. 1174–1186, 2017.
- [28] G. Auer, V. Giannini, C. Desset, I. Godor, P. Skillermark, M. Olsson, M. A. Imran, D. Sabella, M. J. Gonzalez, O. Blume *et al.*, "How much energy is needed to run a wireless network?" *IEEE wireless communications*, vol. 18, no. 5, pp. 40–49, 2011.
- [29] A. A. Razzac, T. Chahed, Z. Shamseddine, and W. Zahwa, "Advanced sleep modes in 5G multiple base stations using non-cooperative multi-agent reinforcement learning," in *GLOBECOM 2023-2023 IEEE Global Communications Conference*. IEEE, 2023, pp. 7025–7030.
- [30] 3GPP, "Study on channel model for frequencies from 0.5 to 100 ghz," 3rd Generation Partnership Project (3GPP), Technical Report 38.901.
- [31] 3GPP, "User Equipment (UE) radio access capabilities," 3GPP TS 38.306, version 16.2.0, 2020.
- [32] —, "Study on integrated access and backhaul," 3GPP TR 38.874, version 16.0.0, 2018.
- [33] H. P. Williams, *Model building in mathematical programming*. John Wiley & Sons, 2013.
- [34] D. Kirov, P. Nuzzo, R. Passerone, and A. Sangiovanni-Vincentelli, "Optimized selection of wireless network topologies and components via efficient pruning of feasible paths," in *Proceedings of the 55th Annual Design Automation Conference*, 2018, pp. 1–6.
- [35] G. Barlacchi, M. De Nadai, R. Larcher, A. Casella, C. Chitic, G. Torrisi, F. Antonelli, A. Vespignani, A. Pentland, and B. Lepri, "A multi-source dataset of urban life in the city of Milan and the Province of Trentino," *Scientific data*, vol. 2, no. 1, pp. 1–15, 2015.
- [36] P. Testolina, M. Polese, and T. Melodia, "Sharing spectrum and services in the 7–24 GHz upper midband," *IEEE Communications Magazine*, vol. 62, no. 8, pp. 170–177, 2024.
- [37] S. Kang, M. Mezzavilla, S. Rangan, A. Madanayake, S. B. Venkatakrishnan, G. Hellbourg, M. Ghosh, H. Rahmani, and A. Dhananjay, "Cellular wireless networks in the upper mid-band," *IEEE Open Journal of the Communications Society*, 2024.
- [38] G. Gemmi, R. L. Cigno, and L. Maccari, "On cost-effective, reliable coverage for los communications in urban areas," *IEEE Transactions on Network and Service Management*, vol. 19, no. 3, pp. 2767–2779, 2022.
- [39] 3GPP, "Study on scenarios and requirements for next generation access technologies," 3GPP TR 38.913, 04 2022, version 17.0.0, 2022.
- [40] A. Baiocchi, L. Chiaraviglio, F. Cuomo, and V. Salvatore, "Joint management of energy consumption, maintenance costs, and user revenues in cellular networks with sleep modes," *IEEE Transactions on Green Communications and Networking*, vol. 1, no. 2, pp. 167–181, 2017.
- [41] H. Li, X. Tang, D. Zhai, R. Zhang, B. Li, H. Cao, N. Kumar, and A. Almogren, "Energy-efficient deployment and resource allocation for O-RAN-enabled UAV-assisted communication," *IEEE Transactions on Green Communications and Networking*, 2024.
- [42] T. Q. Quek, W. C. Cheung, and M. Kountouris, "Energy efficiency analysis of two-tier heterogeneous networks," in *17th European Wireless 2011-Sustainable Wireless Technologies*. VDE, 2011, pp. 1–5.